

The orthotropic viscoelastic behavior of aortic elastin

Yu Zou · Yanhang Zhang

Received: 11 May 2010 / Accepted: 25 September 2010
© Springer-Verlag 2010

Abstract In this paper, we studied the viscoelastic behaviors of isolated aortic elastin using combined modeling and experimental approaches. Biaxial stress relaxation and creep experiments were performed to study the time-dependent behavior of elastin. Experimental results reveal that stress relaxation preconditioning is necessary in order to obtain repeatable stress relaxation responses. Elastin exhibits less stress relaxation than intact or decellularized aorta. The rate of stress relaxation of intact and decellularized aorta is linearly dependent on the initial stress levels. The rate of stress relaxation for elastin increases linearly at stress levels below about 60 kPa; however, the rate changes very slightly at higher initial stress levels. Experimental results also show that creep response is negligible for elastin, and the intact or decellularized aorta. A quasi-linear viscoelasticity model was incorporated into a statistical mechanics based eight-chain microstructural model at the fiber level to simulate the orthotropic viscoelastic behavior of elastin. A user material subroutine was developed for finite element analysis. Results demonstrate that this model is suitable to capture both the orthotropic hyperelasticity and viscoelasticity of elastin.

Keywords Elastin · Viscoelasticity · Orthotropic hyperelasticity · Constitutive model · Biaxial tensile test · Stress relaxation

1 Introduction

As one of the major extracellular matrix (ECM) components, elastin is essential to accommodate physiological

deformation and provide elastic support for blood vessels. Elastin degradation is greatly associated with loss in compliance and stiffening in the arterial wall, which presents in many cardiovascular diseases including diabetes, hypertension, aortic aneurysm, and atherosclerosis (Campa et al. 1987; Chung et al. 2009; Cameron et al. 2003; Agabiti-Rosei et al. 2009; Boutouyrie et al. 2008; Diez 2007; Uitto 1979; Satta et al. 1998). Degradation of elastin in the artery has been assumed to be a major cause that alters the stress distribution produced by blood pressure (MacSweeney et al. 1992, 1994; Silver et al. 2001).

Elastin degradation and failure greatly compromises the mechanical properties of blood vessels. The mechanical properties of elastin have been studied in the past three decades owing to its importance on the functionality of many connective tissues (Lyerla and Torchia 1975; Gosline 1976; Lillie and Gosline 1990; Daamen et al. 2007; Gundiah et al. 2007, 2009; Lillie and Gosline 2007; Zou and Zhang 2009). However, the time-dependent properties of elastin and its involvement in physiological functions and diseases remain to be understood. The viscoelastic properties of elastin are closely related to its microstructure, hydration level, pressure, temperature, and the external mechanical and chemical environments (Lillie and Gosline 1990, 2002; Weinberg et al. 1995; Spina et al. 1999). Elastin in the medial layer of arteries consists of hydrated elastin fibers that are approximately 3 μm in diameter, which are assembled into the lamellar structures at the microscopic level (Winlove and Parker 1990). In previous work, molecular probe techniques have been used to characterize the organization of isolated elastin (Weinberg et al. 1995). The fibers were found to contain a network of water-filled pores accessible to solutes with molecular weights below 1,000 daltons. The water spaces between and around fibrils are accessible to much larger solutes. The intra- and extrafibrillar compartments can be

Y. Zou · Y. Zhang (✉)
Department of Mechanical Engineering, Boston University,
110 Cummington Street, Boston, MA 02215, USA
e-mail: yanhang@bu.edu

modified by mechanical stresses, chemical environment, osmotic pressure, and temperature (Weinberg et al. 1995). When subjected to external stress, elastin molecules rearrange. The relaxation time required for the rearrangement is directly related to the free volume available for the molecular chains to move (Lillie and Gosline 1996; Knauss and Emri 1981).

In a few previous studies on the time-dependent mechanical behavior of elastin, loading has been limited to uniaxial stretching (Weinberg et al. 1995; Silver et al. 2001; Lillie and Gosline 1996, 2002), which ignores the multiaxial loading state under physiological conditions and thus the intrinsic anisotropic properties of soft tissue. Under physiological conditions, aortas are subjected to cyclic strains in both circumferential and longitudinal directions due to the normal and shear forces exerted by pulsatile blood flow. Planar biaxial tensile test with independent control of load in both perpendicular directions has been used broadly to study the mechanical behavior of various soft biological tissues (Sacks and Sun 2003; Geest et al. 2006; Knezevic et al. 2002; Zou and Zhang 2009; Jhun et al. 2009). Although it cannot replicate the physiological loading conditions, biaxial tensile test is sufficient on elucidating the anisotropic mechanical properties of soft tissues with plane stress assumptions. Such capabilities make it a useful tool for in vitro understanding of tissue mechanics and for determining material parameters in sophisticated constitutive models.

It is commonly accepted that for soft biological tissues, the initial loading curves are substantially different from the subsequent loading curves (Fung 1993), which makes preconditioning an important step in order to obtain a repeatable stress–strain response of soft tissues (Sauren et al. 1983; Carew et al. 2000). However, preconditioning has often been limited to studies on the elastic behaviors of soft biological tissues. Carew et al. (2004) found that porcine aortic valve can only exhibit repeatable stress relaxation curves when they are subjected to at least 5 cycles of repeated stress relaxation test. A recent study found that ligaments have good repeatability for both elastic and stress relaxation tests (Öhman et al. 2009). Despite the discrepancy, to the best of our knowledge no study has been conducted to assess the repeatability of stress relaxation behavior of blood vessels and ECM.

Incorporation of viscoelasticity into constitutive models will introduce additional material parameters, thus modeling the time-dependent behavior of soft tissue adds an additional level of computational complexity. Several general techniques have been proposed in the literature to model the viscoelastic behavior of soft tissue. State variable approach introduced a set of state variables to model the nonlinear inelastic process (Holzapfel et al. 2002). Biphase model that includes both solid and interstitial fluid phases was developed for modeling the time-dependent behavior of cartilage (Mow et al. 1980; Soulhat et al. 1999). The rheological

network formulation incorporating a discrete number of elastic and viscous elements in parallel and/or in series was applied to model the viscoelastic behavior of elastomers (Bergstrom and Boyce 2001) and biological soft tissue (Bischoff et al. 2004). The quasi-linear viscoelasticity (QLV) theory was introduced into the biomechanical literature by Fung (1993). This model is characterized by an instantaneous elastic stress response and a relaxation function. Due to its relative ease to implement as well as the limited number of material parameters required to model the viscoelastic response of soft tissue, the theory of QLV has been widely implemented to model the viscoelastic response of soft biological tissues (Kwan et al. 1993; Carew et al. 1999; Sverdluk and Lanir 2002; Doebling et al. 2004; Bischoff 2006; Giles et al. 2007).

In this study, the viscoelastic behaviors of healthy aortic elastin were studied using combined experimental and modeling approaches. Biaxial stress relaxation and creep experiments were performed to study the time-dependent behavior of elastin. Preconditioning of stress relaxation on elastin was investigated. QLV model was incorporated into a statistical mechanics based eight-chain microstructural model to describe the orthotropic viscoelastic behavior of aortic elastin.

2 Materials and methods

2.1 Sample preparation

Thoracic aortas were harvested from pigs (12–24 months; 160–200 lb) at a local abattoir and transported to the laboratory on ice. Before experiments, the aortas were cleaned off adherent tissues and fat and rinsed in distilled water. Thoracic aortas of similar sizes were chosen for experiments. Samples of about 20 × 20 mm were cut at about the midpoint of the thoracic aorta. All samples were taken from the same longitudinal region of the aorta to avoid changes in mechanical properties with aortic longitudinal position. Experiments on aortas were performed within one hour from delivery. Isolated elastin was obtained using a cyanogen bromide (CNBr) treatment (Lu et al. 2004), following procedures described in our previous study (Zou and Zhang 2009). Briefly, aortic samples were treated in 50 mg/mL CNBr (Acros Organics) in 70% formic acid (Acros Organics) solution with gentle stirring for 19 h at room temperature. They were then stirred in the same solution for 1 h at 60 °C, followed by 5-min boiling. Decellularized ECM was obtained using Triton X-100 decellularization process (Bader et al. 1998). Aortic samples were subjected to continuous shaking in a solution of 1% Triton X-100 (Bio-Rad) with 0.2% EDTA in hypotonic Tris buffer (10 mM Tris, pH 8.0) for 48 h,

together with RNase A (20 $\mu\text{g/ml}$) and DNase (0.2 mg/ml). Dimensions of aorta, decellularized ECM, and elastin tissue samples were measured and recorded for further experiments and stress calculation. The length and width of the sample were measured using a digital caliper. The thickness of the each tissue sample was measured at six different locations across the sample and averaged. The tissue samples were kept in 1X phosphate buffered saline (PBS) for further experiment. All the chemicals were purchased from Fisher Scientific unless otherwise specified.

2.2 Scanning electron microscopy (SEM)

SEM was performed on the cross sections of tissue samples to examine the morphology using a JOEL JSM-6100 SEM machine operated at 5kv. Before SEM, the samples were fixed in Karnovsky's fixative kit (2% paraformaldehyde, 2.5% glutaraldehyde, and 0.1M sodium phosphate buffer, Fisher Scientific) for 1 h. The fixed samples were then dehydrated in a series of graded ethanol of 50, 70, 85, and 100%. The samples were then dried using Denton vacuum DCP-1 CO_2 critical point dryer. A 20-nm thin layer of platinum was coated on the cross section of the samples using Cressington 108 Sputter Coater.

2.3 Histology

Histology studies were performed to confirm the removal of cells in the decellularized ECM, and collagen and other ECM components in the isolated elastin. Tissue samples were fixed in 10% formalin buffer and then embedded in paraffin. Thin sections of about 6 μm in thickness were cut for histological stain. Tissue samples with Movat's pentachrome stain were examined for the presence of cells, elastin, and collagen. Alcian blue stain (PH=2.5) was also performed to confirm the removal of glycosaminoglycans (GAGs) in isolated elastin.

2.4 Biaxial tensile testing

A biaxial tensile testing device was used to perform biaxial stress relaxation and creep tests. This device has been used in our previous study on the anisotropic mechanical behavior of elastin (Zou and Zhang 2009). Briefly, tissue samples of about 2 cm in square were sutured at the sides, and an equi-biaxial membrane tension was applied to the sample. All biaxial tensile tests of elastin were performed in 1X PBS at room temperature following test protocols. The aorta and decellularized ECM were also tested for comparison. Before stress relaxation or creep tests, tissue samples were preconditioned for 8 cycles of quasi-static tensile tests with 15 s of half cycle time equi-biaxially to obtain repeatable material response. This preconditioning test began from

an initial 3 g tare load to the peak membrane tension to be applied in the following stress relaxation or creep tests. The peak membrane tension varied from 20 to 160N/m.

For stress relaxation test, equibiaxial tension was applied to the sample following the preconditioning protocols. Immediately after, the sample was quickly stretched to the target stretch with a rise time of 2 s and held at this constant stretch for 1,800 s. For creep test, after the last cycle of equibiaxial tension, the tissue sample was quickly loaded, and the tension was kept constant for 1,800 s. The tension and stretch in both loading directions were recorded during the holding period. In repeatability tests, five cycles of stress relaxation and creep tests were performed on each sample to confirm the repeatability of the viscoelastic behavior. To study the dependence on initial stress level, repeatability tests were first performed to achieve repeatable stress relaxation properties, the sample was then tested under different initial stresses. The sequence of initial stress levels is random. Cauchy stress σ (Zou and Zhang 2009) and Green-Lagrange strain E (Humphrey 2002) were calculated and used to describe the mechanical behavior of elastin.

2.5 Constitutive modeling

In the present study, one-dimensional QLV model was incorporated into a statistical mechanics based orthotropic hyperelastic model (Bischoff et al. 2002) implemented previously by Zhang et al. (2005) for the study of the mechanics of aortic elastin (Zou and Zhang 2009). This three-dimensional orthotropic viscoelastic model was used to simulate the time-dependent mechanics of elastin. Finite element implementation of the model was realized using discrete spectrum approximation (Puso and Weiss 1998).

2.5.1 Incorporation of fiber-level viscoelasticity for the tissue-level time-dependent behavior

The QLV model was firstly incorporated into a single freely jointed chain. The viscoelastic chain stress was then incorporated into a network composed of eight-chain unit elements to model the orthotropic viscoelastic behavior at the tissue level (Bischoff 2006). According to the QLV theory, the general form of the second Piola-Kirchhoff (2nd P-K) stress $\mathbf{S}(t)$ is given by (Fung 1993):

$$\mathbf{S}(t) = \int_0^t G(t-\tau) \frac{\partial \mathbf{S}^e}{\partial \tau} d\tau \quad (1)$$

In Eq. (1), \mathbf{S}^e is the elastic stress function and $G(t)$ is the reduced relaxation function:

$$G(t) = \frac{1 + C[E_1(t/\tau_2) - E_1(t/\tau_1)]}{1 + C \ln(\tau_2/\tau_1)} \quad (2)$$

where C , τ_1 , and τ_2 are material parameters and $E_1(z)$ is the exponential integral function defined by $E_1(z) = \int_z^\infty \frac{e^{-t}}{t} dt$ ($|\arg z| < \pi$).

The macroscopic strain energy function of the eight-chain orthotropic hyperelastic model is given by (Zhang et al. 2005; Bischoff et al. 2002):

$$W = \frac{nk\Theta}{4} \left[N \sum_{i=1}^4 \left(\frac{\rho^i}{N} \beta_\rho^i + \ln \frac{\beta_\rho^i}{\sinh \beta_\rho^i} \right) - \frac{\beta_p}{\sqrt{N}} \ln \left(\lambda_a^2 \lambda_b^2 \lambda_c^2 \right) \right] + B [\cosh(J - 1) - 1] + W_0 \tag{3}$$

where W is the overall strain energy function, n is the chain density per unit volume, and N is the number of rigid links within each chain. Parameters a , b , and c , normalized by the length of rigid links, are dimensions of the unit element along the principal material directions \mathbf{a} , \mathbf{b} , and \mathbf{c} , respectively. λ_a , λ_b , and λ_c are stretches along these directions. $p = \frac{1}{2} \sqrt{a^2 + b^2 + c^2}$ is the undeformed normalized length of each chain, and ρ^i is the normalized deformed length of the i -th chain. $\beta_p = \ell^{-1}(p/N)$, and $\beta_\rho^i = \ell^{-1}(\rho^i/N)$ are the inverse Langevin functions. k is Boltzmann’s constant ($k = 1.38 \times 10^{-23} \text{J/K}$), and Θ is the absolute temperature. B is a parameter controlling the bulk compressibility. It is assumed to be much greater than the initial stiffness $nk\Theta$ in order to model the nearly incompressibility of soft tissue. J is the volume ratio. The elastic 2nd P-K stress tensor \mathbf{S}^e can be obtained by:

$$\mathbf{S}^e = \frac{\partial W}{\partial \mathbf{E}} = \frac{n}{4} \left[\sum_{i=1}^4 \mathbf{S}_{\text{chain}}^e - k\Theta \frac{\beta_p}{\sqrt{N}} \left(\frac{a^2}{\lambda_a^2} \mathbf{a} \otimes \mathbf{a} + \frac{b^2}{\lambda_b^2} \mathbf{b} \otimes \mathbf{b} + \frac{c^2}{\lambda_c^2} \mathbf{c} \otimes \mathbf{c} \right) \right] + BJ\mathbf{C}^{-1} \sinh(J - 1) \tag{4}$$

where \mathbf{C} is the right Cauchy-Green tensor and $\mathbf{C} = \mathbf{F}^T \mathbf{F}$, $\mathbf{E} = \frac{1}{2}(\mathbf{C} - \mathbf{I})$ is the Green-Lagrange strain tensor, and \mathbf{F} is the deformation gradient. $\mathbf{S}_{\text{chain}}^e$ is the elastic 2nd P-K stress of a single freely jointed chain and is given by:

$$\mathbf{S}_{\text{chain}}^e = k\Theta \frac{\mathbf{p}^i \otimes \mathbf{p}^i}{\rho^i} \beta_{\rho^i} \tag{5}$$

where \mathbf{p}^i is the normalized chain vector describing the undeformed chain.

To model the tissue-level time-dependent behavior, the elastic chain stress $\mathbf{S}_{\text{chain}}^e$ in Eq. (4) is replaced by the viscoelastic chain stress according to the QLV formulation.

The resulting viscoelastic stress tensor \mathbf{S} in the macroscopic continuum model is then described as:

$$\mathbf{S} = \frac{n}{4} \left[\sum_{i=1}^4 \int_0^t G(t - \tau) \frac{\partial (\mathbf{S}_{\text{chain}}^e)}{\partial \tau} d\tau - k\Theta \frac{\beta_p}{\sqrt{N}} \left(\frac{a^2}{\lambda_a^2} \mathbf{a} \otimes \mathbf{a} + \frac{b^2}{\lambda_b^2} \mathbf{b} \otimes \mathbf{b} + \frac{c^2}{\lambda_c^2} \mathbf{c} \otimes \mathbf{c} \right) \right] + BJ\mathbf{C}^{-1} \sinh(J - 1) \tag{6}$$

2.5.2 Finite element implementation

For finite element implementation, the viscoelastic stress, which is specified by the history of deformation, is evaluated using numerical integration algorithm. The reduced relaxation function in Eq. (2) is approximated by a series of exponential functions and can be written as (Puso and Weiss 1998):

$$G(t) = G_e + \frac{G_0 - G_e}{N_d + 1} \sum_{l=0}^{N_d} \exp(-t/10^{(l+I_0)}) \tag{7}$$

where G_e , G_0 , N_d , and I_0 are material parameters that will be obtained by fitting the simulation results to the experimental stress relaxation data.

Based on the approximated reduced relaxation function in Eq. (7), the viscoelastic stress at time $t + \Delta t$ can be evaluated based on the stress at time t , following Eq. (6):

$$\begin{aligned} & \int_0^{t+\Delta t} G(t + \Delta t - \tau) \frac{\partial \mathbf{S}_{\text{chain},t+\Delta t}^e}{\partial \tau} d\tau \\ &= \int_0^{t+\Delta t} \left[G_e + K \sum_{l=0}^{N_d} \exp\left(-\frac{-(t + \Delta t - \tau)}{v_l}\right) \right] \frac{\partial \mathbf{S}_{\text{chain},t+\Delta t}^e}{\partial \tau} d\tau \\ &= G_e (\mathbf{S}_{\text{chain},t+\Delta t}^e - \mathbf{S}_{\text{chain},t=0}^e) + K \sum_{l=0}^{N_d} \exp\left(-\frac{-\Delta t}{v_l}\right) H_l \\ & \quad + K \sum_{l=0}^{N_d} \exp\left(-\frac{-\Delta t}{v_l}\right) \int_t^{t+\Delta t} \exp\left(-\frac{-(t - \tau)}{v_l}\right) \frac{\partial \mathbf{S}_{\text{chain},t+\Delta t}^e}{\partial \tau} d\tau \end{aligned} \tag{8}$$

where $v_l = 10^{l+I_0}$, $K = \frac{G_0 - G_e}{N_d + 1}$ and $H_l = \int_0^t \exp\left(-\frac{-(t - \tau)}{v_l}\right) \frac{\partial \mathbf{S}_{\text{chain},t}^e}{\partial \tau} d\tau$ which can be obtained from previous time step when $\Delta t = 0$.

In Eq. (8), the first term can be obtained from elastic chain stress; the second term needs to recall the viscoelastic chain stress from the previous time step. An approximation is made

to the third term using the central difference rule so that:

$$\begin{aligned}
 & K \sum_{l=0}^{N_d} \exp\left(\frac{-\Delta t}{v_i}\right) \int_t^{t+\Delta t} \exp\left(-\frac{(t-\tau)}{v_i}\right) \frac{\partial \mathbf{S}_{\text{chain},t+\Delta t}^e}{\partial \tau} d\tau \\
 &= K \sum_{l=0}^{N_d} \exp\left(\frac{-\Delta t}{v_i}\right) \frac{\mathbf{S}_{\text{chain},t+\Delta t}^e - \mathbf{S}_{\text{chain},t}^e}{\Delta t} \\
 &\quad \times \int_t^{t+\Delta t} \exp\left(-\frac{(t-\tau)}{v_i}\right) d\tau \tag{9}
 \end{aligned}$$

In addition to the stress tensor, the fourth-order elasticity tensor \mathbf{H} is needed in order to form the stiffness matrix for finite element analysis. The time-dependent elasticity tensor \mathbf{H} is defined as $\mathbf{H} = 2 \frac{\partial \mathbf{S}(t+\Delta t)}{\partial \mathbf{C}(t+\Delta t)}$, where $\mathbf{C}(t + \Delta t)$ is the right Cauchy-Green deformation tensor at time $t + \Delta t$. For time-dependent analysis, $\mathbf{H}(t + \Delta t)$ can be estimated from (Puso and Weiss 1998):

$$\mathbf{H}(t + \Delta t) = \left[G_e + K \sum_{l=0}^{N_d} \frac{(1 - \exp(-\Delta t/v_i))}{\Delta t/v_i} \right] \times \mathbf{H}(0) \tag{10}$$

where $\mathbf{H}(0)$ is the elasticity tensor at $t = 0$, i.e., the beginning of the holding period. The elasticity tensor $\mathbf{H}(0)$ can be obtained from $\mathbf{H} = 2 \frac{\partial \mathbf{S}^e}{\partial \mathbf{C}}$, where \mathbf{S}^e is the elastic 2nd P-K stress tensor given in (Eq. 4) (Zhang et al. 2005).

The Cauchy stress and elasticity tensor in the deformed configuration can then be achieved by applying a push forward operation (Holzapfel 2000) on Eqs. (6) and (10). A user material subroutine (UMAT) was developed to implement the three-dimensional orthotropic viscoelastic constitutive model in ABAQUS 6.7. The elastic and viscoelastic chain stresses were recorded and stored at every time step for the calculation of viscoelastic chain stress in the next time step. For finite element simulation, a quarter of the sample was modeled due to the symmetric loading conditions in biaxial tensile testing. General-purpose shell elements (S4R) were used with inherent plane stress assumption. Finite element simulation of stress relaxation reflected the experimen-

tal procedure described earlier. During the first time step, shell edge load was applied on the sides of the sample to simulate the biaxial tensile loading. In the second time step, displacements were held constant for about 30 min, and the stress was recorded during the stress relaxation process.

2.6 Statistical analysis

Normalized creep results were expressed as mean \pm standard error of the mean. Comparisons between elastin, aorta, and decellularized ECM samples were made using two-tail two-sample *t*-Test assuming unequal variances. Differences are considered statistically significant when $p < 0.05$.

3 Results

CNBr treatment removes smooth muscle cells, collagen, and other ECM components to obtain the isolated elastin. Triton X-100 decellularization process removes the smooth muscle cells. Decellularization and isolation processes significantly decrease the thickness of the tissue. The average thicknesses for thoracic aorta, decellularized ECM, and elastin samples are (mean \pm SD, $n = 6$ for each tissue type) 1.70 ± 0.20 mm, 1.34 ± 0.12 mm, and 0.78 ± 0.15 mm, respectively. SEM image in Fig. 1a shows that the cross section of isolated elastin consists of concentric layers of elastin sheets, which are less obvious with the presence of collagen fibers and smooth muscle cells in the intact aorta (Fig. 1c). Decellularized ECM (Fig. 1b) preserves the major microstructure of aorta. Removal of both the smooth muscle cells and collagen fibers in elastin is verified by histological images with Movat’s pentachrome stain in Fig. 2a. For the decellularized ECM, only cells are completely removed, as shown in Fig. 2b. Histology image of the intact porcine aorta in Fig. 2c shows a cross-linked network of collagen and elastin fibers with embedded cells. Alcian blue stain (pH = 2.5) was performed to further verify the removal of GAGs in elastin, since GAGs play a crucial role in tissue viscoelasticity (Stephens et al. 2008; Liao and Vesely 2004). Figure 2f shows the

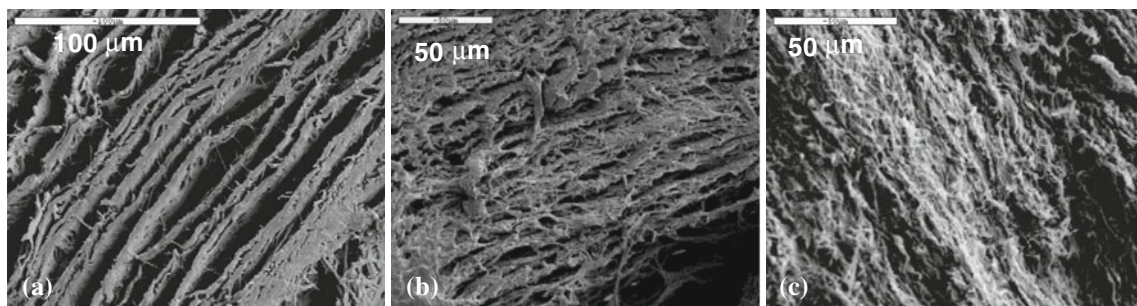


Fig. 1 SEM images of (a) isolated elastin, (b) decellularized ECM, and (c) intact aorta

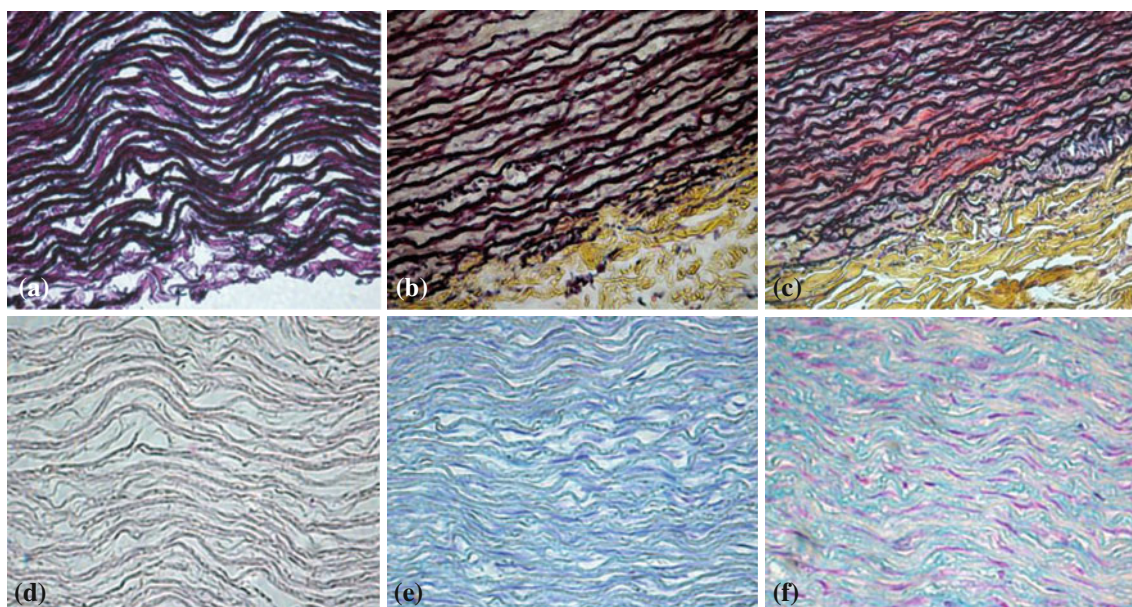


Fig. 2 Histology images of (a, d) isolated elastin, (b, e) decellularized ECM, and (c, f) intact aorta. Movat's pentachrome stains elastin purple-black, collagen yellow, and cells red (a–c). Alcian blue stains GAGs blue and cells pink (d–f)

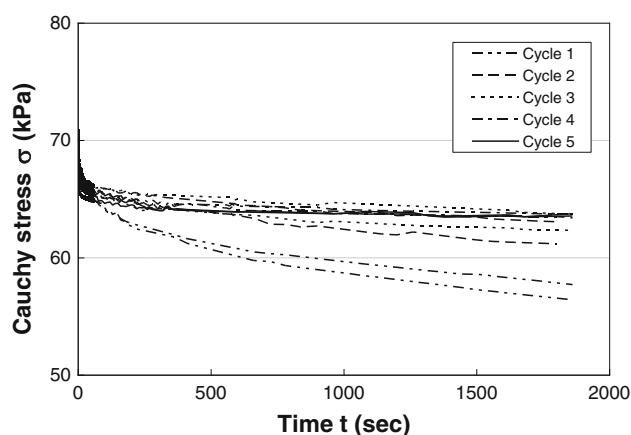


Fig. 3 Representative stress relaxation curves obtained from repeated testing the same elastin sample for five testing cycles. Stress relaxation responses in both circumferential and longitudinal directions are shown

presence of smooth muscle cells, GAGs, and collagen and elastin fibers in the aorta sample. The absence of cells in elastin and decellularized ECM is shown again in Fig. 2d,e. GAGs are preserved in the decellularized ECM but are completely removed in the isolated elastin. Both SEM and histology images of isolated elastin samples exhibit a lower density of fiber network due to the removal of cells and other ECM components.

Multiple stress relaxation tests on samples of elastin ($n = 6$), intact aorta ($n = 7$), and decellularized ECM ($n = 6$) were performed to examine the repeatability of stress relaxation behavior. Figure 3 shows the representative stress relaxation curves obtained from five repeated testing of the same

aortic elastin sample. Elastin exhibits significantly more stress relaxation in the first test. The repeatability is highly improved in the subsequent cycles of stress relaxation tests. Although not shown here, intact aorta and decellularized ECM exhibits similar behavior with the initial stress relaxation curves significantly different from subsequent testing. The repeatability ratio between two curves is defined as the minimum of the ratios of stresses from the more relaxed to the less relaxed curve calculated at 2, 10, 100, 1,000 and 1,800s (Carew et al. 2004). Table 1 shows the repeatability of elastin, aorta, and decellularized ECM. The repeatability of stress relaxation behavior is improved by applying subsequent cycles of stress relaxation tests. The fifth cycle of stress relaxation has raised the repeatability to about 0.99 for all the samples. These results confirm that stress relaxation preconditioning is essential to achieve repeatable stress relaxation behavior in soft biological tissues. The fifth cycle of stress relaxation from all three tissue types has satisfying repeatability and can be used to study the time-dependent mechanical behavior. If not specifically indicated, the stress relaxation results showed in the present study are referred to results from the fifth cycle.

Figure 4 shows the representative biaxial stress relaxation curves of the elastin, intact aorta, and decellularized ECM. All samples were tested at the initial stresses of 101.03 ± 0.72 kPa to eliminate the effect of initial stress levels on the rate of stress relaxation. In order to compare the time-dependent responses of different tissue samples, the stresses were normalized to that at the beginning of the holding period. Over the holding period of half an hour, aorta shows more significant stress relaxation than decellularized ECM

Table 1 Repeatability of stress relaxation tests of elastin, decellularized ECM, and aorta samples

	Cycle 1 vs. 2	Cycle 2 vs. 3	Cycle 3 vs. 4	Cycle 4 vs. 5
Elastin ($n = 6$)	0.9031 ± 0.0164	0.9792 ± 0.0147	0.9783 ± 0.0171	0.9926 ± 0.0054
ECM ($n = 6$)	0.9325 ± 0.0345	0.9668 ± 0.0122	0.9861 ± 0.0096	0.9912 ± 0.0076
Aorta ($n = 7$)	0.9365 ± 0.0257	0.9621 ± 0.0345	0.9790 ± 0.0146	0.9923 ± 0.0089

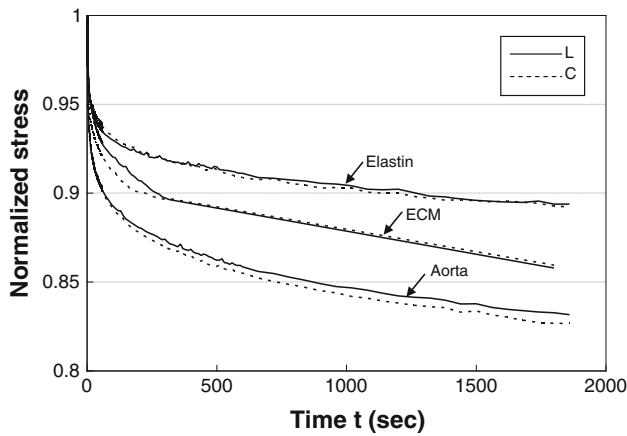


Fig. 4 Representative stress relaxation curves of elastin, decellularized ECM, and intact aorta at initial stresses of 101.03 ± 0.72 kPa. *Solid and dotted lines* represent the stress relaxation behaviors in longitudinal (L) and circumferential (C) directions, respectively

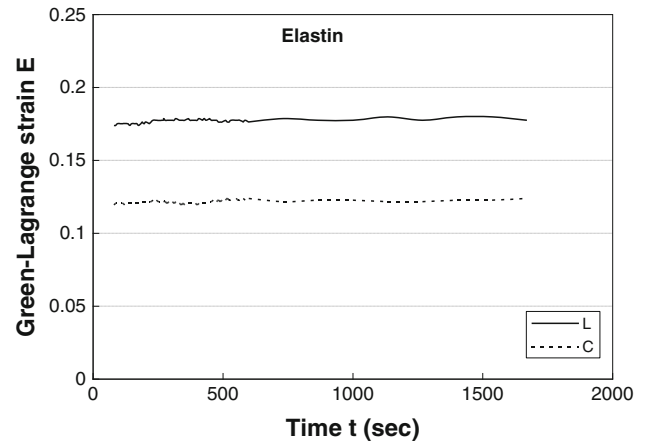


Fig. 5 Representative creep curves of elastin. The circumferential and longitudinal direction has different initial strains due to the anisotropy of the elastin. *Solid and dotted lines* represent the creep behaviors in longitudinal (L) and circumferential (C) directions, respectively

and elastin in both the circumferential and longitudinal directions. Moreover, decellularized ECM shows more stress relaxation than elastin. For all three tissue types, most of the stress relaxation happens during the first 10 min of the holding period.

Representative biaxial creep behavior of elastin is shown in Fig. 5. Under equi-biaxial tension, elastin has higher strain in the longitudinal direction than in the circumferential direction due to the anisotropic mechanical property of the elastin. The results show that the creep behavior is negligible for the elastin. Although not shown here, aorta and decellularized ECM exhibits similar negligible creep behavior as elastin. The normalized maximum creep of elastin, decellularized ECM, and intact aorta ($n = 3$) is $101.6 \pm 1.4\%$, $101.7 \pm 0.5\%$, and $101.7 \pm 1.3\%$, respectively, with no statistically significance and is considered negligible.

The dependence of stress relaxation upon initial stress levels was investigated. Stress relaxation tests were performed at varying stress levels by applying different initial equibiaxial tension to the tissue samples. Each sample was tested at multiple initial stress levels. Figure 6 shows the representative stress relaxation curves for aorta, ECM, and elastin samples at different initial stress levels. To better compare the initial stress level dependence of stress relaxation, the rate of stress relaxation, stress drop rate, at each initial stress level was obtained by taking the slope of the stresses vs. time semi-log plots in Fig. 6. Averaged stress drop rate

between the circumferential and longitudinal directions was taken, although most samples exhibit almost identical stress relaxation responses in both directions. As shown in Fig. 7, multiple stress relaxation tests demonstrate a linear increase in the rate of stress relaxation with higher initial stress for both aorta and decellularized ECM. The rate of stress relaxation for elastin increases linearly at stress levels below about 60 kPa; however, the rate changes very slightly at higher initial stress levels. Creep tests at different initial strain levels were also performed. Elastin, decellularized ECM, and aorta all exhibit negligible creep behavior at various strain levels (results not shown).

In the present study, the QLV model was incorporated into a statistical mechanics-based orthotropic hyperelastic model, which has been developed earlier and demonstrated to be suitable to model the mechanical properties of elastin (Zhang et al. 2005; Zou and Zhang 2009). Figure 8 shows the simulation results of elastic and viscoelastic behavior of elastin. Experimental results were also plotted for the purpose of comparison. The material parameters can be divided into two groups: four independent parameters (a , b , c , and n) describing the orthotropic hyperelastic behavior of elastin and four more parameters (G_e , G_0 , N_d , and I_0) describing the viscoelastic behavior. Note that the eight-chain network model does not represent the actual organization/alignment of the elastin fibers. Here, the orthotropic eight-chain unit

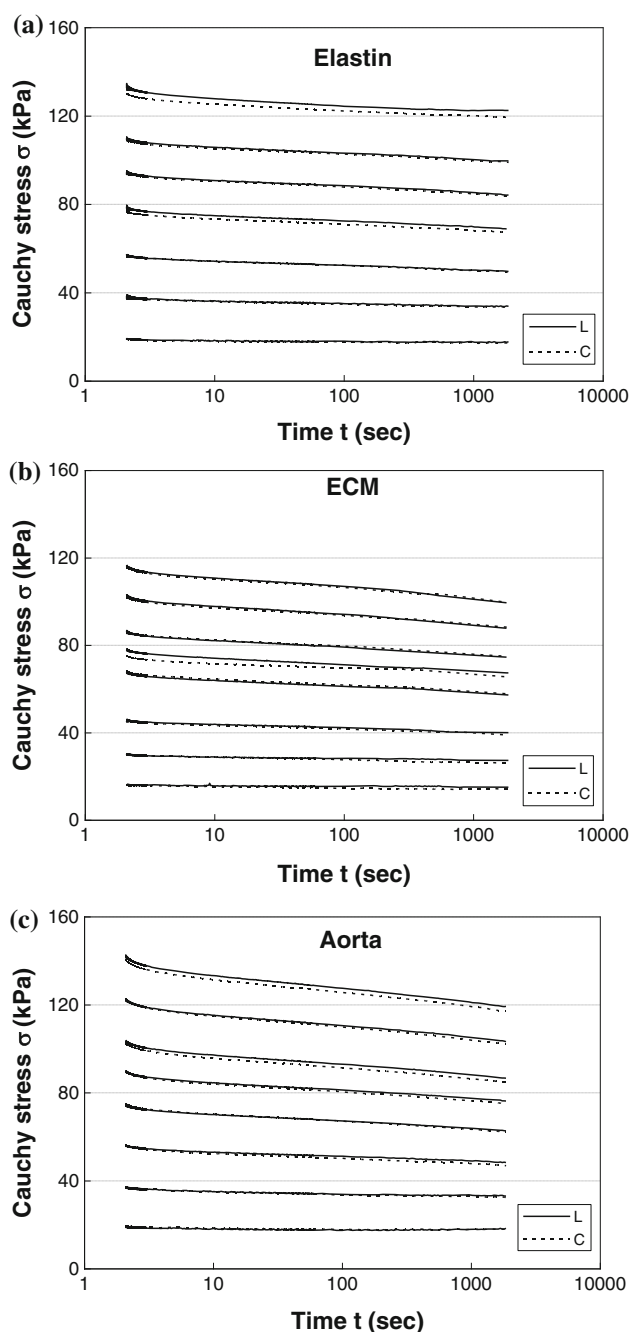


Fig. 6 Representative stress relaxation at different initial stress levels for (a) elastin, (b) decellularized ECM, and (c) intact aorta. *Solid* and *dotted lines* represent the stress relaxation behaviors in longitudinal (L) and circumferential (C) directions, respectively

element is a functional representative in a mechanical sense of the load bearing fibrous network of elastin tissue. The physical meanings of material parameters (a , b , c , and n) and the individual parametric effect on predicting the orthotropic hyperelastic stress–strain responses have been discussed in our previous work (Zou and Zhang 2009). These material parameters were obtained by fitting the simulation

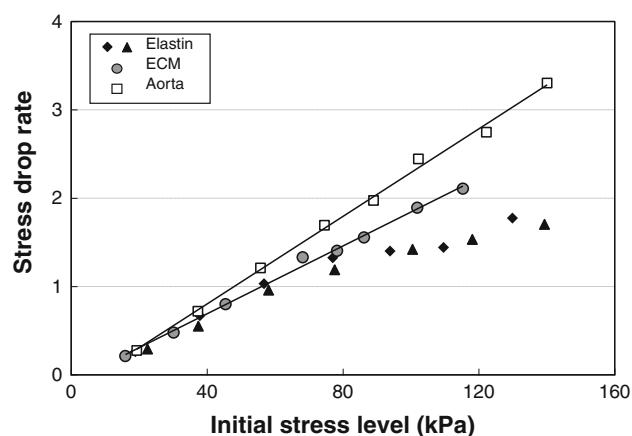


Fig. 7 Stress drop rate as a function of initial stress levels for aorta, decellularized ECM, and elastin samples. Stress drop rate was obtained by taking the slope of the stresses vs. time semi-log plots in Fig. 6 and averaged between the longitudinal and circumferential directions. Linear trend lines were added for aorta and decellularized ECM to aid viewing. The stress drop rates of two elastin samples were presented to better observe the trend

results to the equi-biaxial tensile test data, as shown in Fig. 8a. The viscoelastic material parameters (G_e , G_0 , N_d , and I_0) were obtained by fitting the simulation results to the experimental data from stress relaxation tests, as shown in Fig. 8b. The first and fifth cycles of stress relaxation tests were simulated. Material parameters a , b , c , and n for both cycle tests were kept the same for the description of the orthotropic hyperelastic behavior of elastin. The viscoelastic material parameters were changed assuming that stress relaxation preconditioning only affects the viscoelasticity of elastin. The simulation results fit the experimental data reasonably well for both cycles. These results demonstrate that the orthotropic viscoelastic constitutive model incorporating fiber-level viscoelasticity into the eight-chain statistical mechanics-based microstructural model is suitable to describe the stress relaxation behavior of elastin.

4 Discussions

Our recent study revealed that aortic elastin possesses anisotropic mechanical behavior that is comparable to aorta (Zou and Zhang 2009). In the present study, the viscoelastic properties of elastin were studied using biaxial stress relaxation and creep tests. Stress relaxation preconditioning was performed to examine the repeatability of elastin stress relaxation. Dependence of initial stress levels of elastin's viscoelastic behavior was also investigated. Fiber-level viscoelasticity of elastin fibers incorporated into an orthotropic hyperelastic constitutive model was developed to study the time-dependent mechanics of elastin at the tissue level.

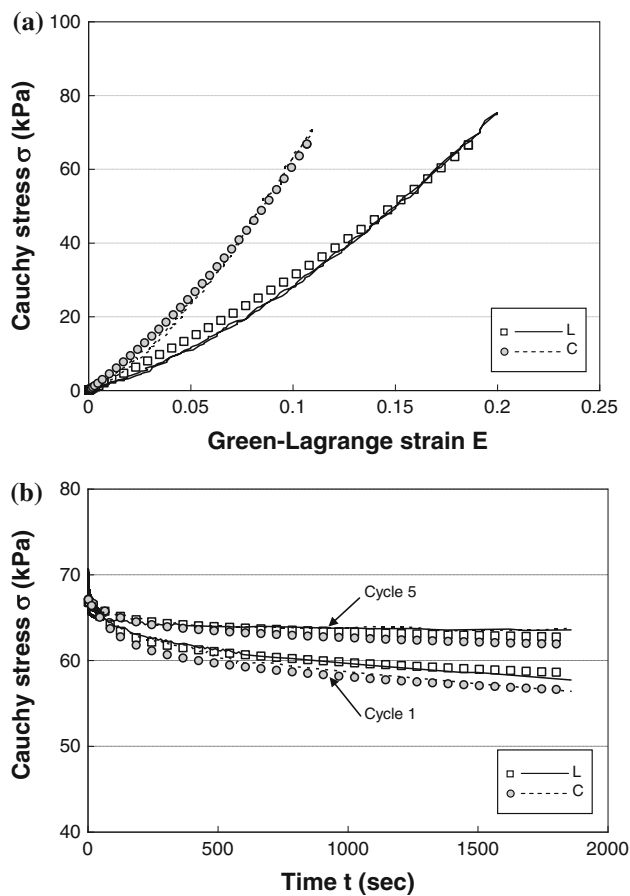


Fig. 8 Simulation results of elastin first subjected to (a) equi-biaxial tensile test, then (b) stress relaxation tests in the first and fifth cycles, represented by *squares* in longitudinal (L) and *circles* in circumferential (C) direction. The corresponding experiment data were also shown for the purpose of comparison and represented by *solid lines* in longitudinal (L) and *dotted lines* in circumferential (C) direction. Material parameters in the simulation are $n = 1.5 \times 10^{16}$ ($1/\text{mm}^3$), $a = 1.386$, $b = 1.67$, $c = 1.3$, $N = 1.6$, $G_e = 0.84$, $G_o = 1.0$, $N_d = 6$, and $I_o = 2$ for the 1st cycle; and $n = 1.5 \times 10^{16}$ ($1/\text{mm}^3$), $a = 1.386$, $b = 1.67$, $c = 1.3$, $N = 1.6$, $G_e = 0.91$, $G_o = 1.0$, $N_d = 6$, and $I_o = 2$ for the 5th cycle

These results will help us understand how the effects of mechanical loading translate into changes in the macroscopic viscoelastic properties of elastin, thus to advance our understanding on the role of microstructural components on vascular remodeling.

Preconditioning has long been adopted to obtain a repeatable stress–strain behavior of soft biological materials. Traditionally, the sample goes through several cycles of loading and unloading, either uniaxially or biaxially for preconditioning (von Maltzahn and Warriyar 1984; Yin et al. 1986; Fung 1993; Carew et al. 2000; Lally et al. 2004). Carew et al. (2004) found that repeatable stress relaxation curves cannot be obtained from this conventional preconditioning method for porcine aortic valve tissues. They suggested at least five cycles of repeated stress relaxation tests would be essential

and sufficient to obtain the repeatability of stress relaxation. Our results show similar phenomena (Fig. 3). For intact porcine aorta, decellularized ECM, and isolated elastin, stress relaxation preconditioning is necessary to ensure repeatable stress relaxation behavior. The first cycle test shows significantly more stress relaxation than the subsequent ones. Through measuring the repeatability ratio between two cycles, the fifth cycle test can generate well-repeatable stress relaxation curves (repeatability ratio > 0.991). The present study was based on the repeatable stress relaxation behavior of elastin, which was expected to be more representative and accurate of the viscoelastic behavior of the three tissue types.

Biaxial stress relaxation tests reveal some interesting facts. The stress relaxation responses of the intact aorta and decellularized ECM are sensitive to the initial stress levels. Our results show that the rate of stress relaxation increases linearly with the initial stress level for intact and decellularized aorta, while for elastin the responses are only stress dependent at stress levels below about 60 kPa. At higher stress levels, elastin becomes almost independent of initial stress levels. Dependence of the magnitude of stress relaxation on initial stress–strain levels has been shown in previous work on the viscoelasticity of ligament (Provenzano et al. 2001; Hingorani et al. 2004). These studies showed that the rate of stress relaxation decreases with higher stress or strain level. They speculated that the decrease in relaxation rate with increasing strain could be the result of the larger strains causing greater water loss, which makes the tissue more elastic and less viscous. A recently study on bladder wall (Nagatomi et al. 2008) reported similar phenomena. Moreover, they observed that the decellularized ECM of bladder wall was insensitive to the initial stress level. They suggested that at lower stress level, more load is carried by the smooth muscle component, while at the higher stress level the ECM is recruited to carry more of the load. The discrepancy between our results and previous findings might due to the differences in composition of biological tissues. Unlike ligament which is collagen dominant, the aorta is an elastic artery with elastin composed up to 30.1% of the total weight (Humphrey 2002). It is well accepted that elastin is responsible for the linear elastic response of blood vessels at lower strains. While at higher strains, the aorta becomes much stiffer in both directions due to the strain stiffening and the involvement of collagen fibers (Cox 1978; Fonck et al. 2007; Lally et al. 2004). Our previous work (Zou and Zhang 2009) further validated that elastin is responsible for the linear elastic response of blood vessels under lower stress. Silver et al. (2001) have suggested that collagen fibers are relaxed at the lower stress state, but at the higher stress state, collagen fibers are uncrimped and start to take load. We speculate that during stress relaxation test of aorta at lower stress or strain level, more load is carried by elastin fibers, while at higher initial stresses, collagen fibers become the major mechanical

component that carry more of the overall load. The shift of mechanical roles between the two major ECM components results in more stress relaxation at higher initial strains for aorta and decellularized ECM.

Figure 4 compared the stress relaxation behavior of three tissue types at stress level of about 100 kPa, which has close physiological relevance. Circumferential stresses in pig aortas at 100 mmHg are around 95–120 kPa (Guo and Kassab 2004 and Stergiopoulos et al. 2001). Previous work showed that collagen fibers are generally recruited only around physiological loads (Silver et al. 2001; Lally et al. 2004; Fonck et al. 2007). Aorta exhibits the most obvious stress relaxation than elastin and decellularized ECM due to the involvement of collagen and smooth muscle cells. It is well recognized that elastin relaxes much less compared with smooth muscle cells or collagen (Fung 1993). In a previous study on urinary bladder wall (Nagatomi et al. 2004), the amount of stress relaxation has been demonstrated to correlate with collagen content. Different stress relaxation responses between elastin and collagen were explained that elastin is easily to be distended under small loads and does not dissipate stored energy as readily as collagen and smooth muscle cells. Our results further demonstrate that elastin relaxes much less than intact aorta or decellularized ECM. Moreover, our study shows that decellularized ECM exhibits less stress relaxation than intact aorta due to the absence of smooth muscle cells. Smooth muscle has a tremendous relaxation though its elastic modulus is low (Fung 1993). Nagatomi et al. (2008) showed that decellularized bladder wall tissue relaxes significantly less than intact bladder due to the lack of smooth muscle cells. A recent study by Williams et al. (2009) demonstrated that the viscoelastic characteristics of intact and decellularized carotid arteries are similar. The stress level of stress relaxation was not reported. It is possible that in their study stress relaxation was performed at low stress level, so that the difference in stress drop rate between intact and decellularized aorta is small. Also, storage of intact aortas at -20°C might cause a loss of smooth muscle cell integrity which might account for the similarity in stress relaxation between the ECM and aorta samples in their study.

Compared with the stress relaxation results, the creep behaviors of aorta, decellularized ECM, and elastin samples are negligible in both the circumferential and longitudinal directions (Fig. 5). This phenomenon has also been observed in earlier studies of soft biological tissues including mitral valve anterior leaflet (Grashow et al. 2006; Liao et al. 2007) and aortic heart valve leaflet (Stella et al. 2007). The present study is the first to show that isolated aortic elastin had very little creep compared with its obvious stress relaxation. Grashow et al. (2006) put forward that complete lack of creep appears to be unique in soft biological tissues and has a functionally independent mechanism as stress relaxation behavior. Recently, a “locked-up” fibril network explanation was

brought by Liao et al. (2007). They proposed that as a result of the stress re-distributed to noncollagenous ECM under constant strain conditions, it allows for stress reduction under constant strain and prevents strain increasing under constant stress conditions. Stella et al. (2007) suggested that fibers are allowed to rotate in a time-dependent manner to achieve a state of reduced fiber stress in the uniaxial creep testing; however, during biaxial creep test, there are no unconstrained segments of the sample due to a lack of time-dependent changes in fiber orientation.

Less creep than stress relaxation has been observed in studies of ligament (Thornton et al. 1997; Provenzano et al. 2001; Hingorani et al. 2004) and corneas (Boyce et al. 2007; Nagatomi et al. 2008). Thornton et al. (1997) suggested that the paradoxical observation between creep and stress relaxation behavior may be explained by the functionally independent mechanisms of these time-dependent behaviors. Stress relaxation response is corresponding to a discrete group of fibers being recruited at prescribed constant elongation, while creep is corresponding to fibers being progressively recruited at constant stress. Their later study (Thornton et al. 2001) incorporated fiber recruitment in structural model which could predict creep from stress relaxation behavior. They suggested that the differences in the stress relaxation and creep behavior in ligaments were explained as a result from the different ways of recruiting relaxing fibers. The gradual recruitment of crimped fibers provides a protective function to reduce creep. The lack of creep can also due to the variation of fibril-ECM interactions, such as the proteoglycan–collagen interactions (Grashow et al. 2006; Stella et al. 2007). Our biaxial creep results show no creep for aorta, decellularized ECM, and elastin samples, which also suggests that stress relaxation and creep depend on functionally different mechanisms. However, more researches are needed to fully understand the separate functions and relations of creep and stress relaxation.

QLV theory has been widely used to model the viscoelastic response of soft tissue, including ligaments (Provenzano et al. 2001), tendons (Johnson et al. 1994; Atkinson et al. 1999), heart valves (Carew et al. 1999), bladders (Nagatomi et al. 2004), and skeletal muscle (Best et al. 1994). Nagatomi et al. (2004) evaluated the viscoelastic properties of normal and spinal cord injured rat bladders. The reduced relaxation function in the circumferential and longitudinal directions was fitted to the tissue stress relaxation responses to determine the material parameters. Giles et al. (2007) incorporated QLV into an exponential model to examine the anomalous rate dependence of the preconditioned response of porcine dermis during load controlled deformation. Bischoff (2006) incorporated the QLV model into a fiber-based orthotropic hyperelastic constitutive model for the study of tissue-level viscoelastic behavior. Similar approach has been adopted in the present study.

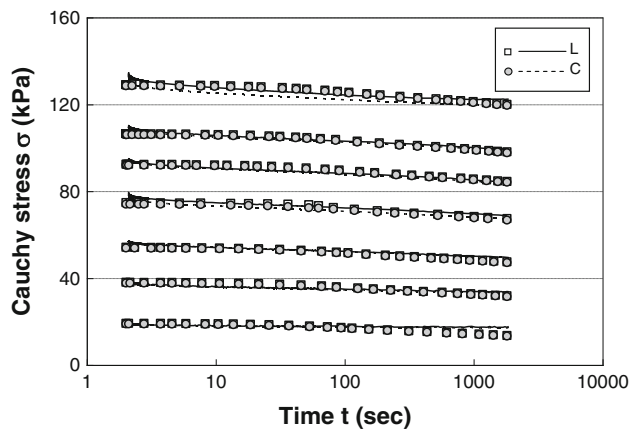


Fig. 9 Simulation results of stress relaxation responses of elastin at different initial stress levels, represented by *squares* in longitudinal (L) and *circles* in circumferential (C) direction. The corresponding experiment data were also shown for the purpose of comparison and represented by *solid lines* in longitudinal (L) and *dotted lines* in circumferential (C) direction. Material parameters for all the simulations are $n = 1.75 \times 10^{16}$ (1/mm³), $a = 1.53$, $b = 1.54$, $c = 1.3$, $N = 1.6$, $G_e = 0.89$, $G_o = 1.0$, $N_d = 6$, and $I_o = 2$

Although the simulation results fit the experimental data reasonably well, the deficiencies associated with the orthotropic viscoelastic constitutive model incorporating fiber-level viscoelasticity using a QLV model should be noted. Since QLV model assumes a separate strain and time dependence of the stress response, it is incapable to simulate the initial stress dependent behavior of stress relaxation. Therefore, a fit for stress relaxation test based on one stress–strain level would predict the same stress relaxation rate for all strains. Such characteristics will limit the usage of QLV model in studies where the viscoelasticity of the aorta or decellularized ECM is concerned. However for elastin, as shown in Fig. 9, since the dependence of the rate of stress relaxation on the initial stress level is small at physiological load, the material parameters fitted from one test can be used to simulate the stress relaxation behavior of elastin under different initial stress levels and provide reasonable predictions. QLV model is also found to be insufficient to characterize the creep behavior of soft tissues due to its intrinsic assumptions on separable strain and time dependence of the stress response (Thornton et al. 1997; Boyce et al. 2007; Nguyen et al. 2008). Despite the deficiencies of QLV model, the negligible creep behavior and less initial stress dependence of stress relaxation behavior of elastin make this present model still adequate to investigate the mechanics of elastin.

There are several limitations in the current study calling for further investigations into the issue. Microstructure studies are lacking to relate the effect of mechanical loading on viscoelasticity. The different mechanisms of stress relaxation and creep behavior are not fully understood, which requires further exploration. Microscopy imaging is needed to better understand the microstructure change of elastin network

during deformation and explore the mechanisms of stress relaxation and creep. Besides, although the material parameters describing the orthotropic hyperelasticity in the constitutive model have physical meanings and could be related to the microstructure of elastin, the QLV model for fiber-level viscoelasticity is phenomenological and lacks structural connections. Due to current experimental device limitations, all the experiments were performed at room temperature and not at 37°C. The mechanical behaviors of soft tissues are temperature dependent (Guinea et al. 2005). However, previous study demonstrated weak temperature effect on the passive mechanical behavior of arterial wall below 60°C (Kang et al. 1995). Recent study showed that the viscoelastic properties of tendons are not sensitive to temperature over short durations between room temperature and 37°C (Huang et al. 2009). Although temperature dependency is not considered in this study, we expect that the relative responses in the three tissue types would be the same at 37°C.

5 Conclusions

To the best of our knowledge, the present study is the first to investigate the time-dependent behavior of elastin using biaxial stress relaxation and creep tests. Our findings provide fundamental understandings on the viscoelasticity of aortic elastin. Such understandings shed light on the role of elastin on controlling the mechanical properties of blood vessels and are essential for future studies on vascular remodeling that involves elastin degradation and failure. The time-dependent mechanics of aortic elastin under biaxial stress relaxation and creep testing were studied using a combination of experimental and theoretical method. Multiple stress relaxation preconditioning was performed to obtain repeatable stress relaxation behavior. Elastin shows less stress relaxation behavior than intact or decellularized aorta samples. The stress relaxation response of elastin is stress level dependent at stress levels below 60 kPa but becomes nearly independent at high stress levels. However, the creep response is negligible for both elastin, and the intact or decellularized aorta samples. The orthotropic viscoelastic constitutive model incorporating fiber-level viscoelasticity through QLV model into an eight-chain statistical mechanics-based microstructural orthotropic model is suitable to describe both elastic and viscoelastic responses of elastin.

Acknowledgments This work was supported in part by funding from NSF Grants 0700507, CAREER 0954825, and the College of Engineering at Boston University.

References

- Agabiti-Rosei E, Portei E, Rizzoni D (2009) Arterial stiffness, hypertension, and rational use of nebivolol. *Vasc Health Risk Manag* 5:353–360

- Atkinson TS, Ewers BJ, Haut RC (1999) The tensile and stress relaxation responses of human patellar tendon varies with specimen cross-sectional area. *J Biomech* 32:907–914
- Bader A, Schilling T, Teebken OE, Brandes G, Herden T, Steinhoff G, Haverich A (1998) Tissue engineering of heart valves-human endothelial cell seeding of detergent acellularized porcine valves. *Eur J Cardiothorac Surg* 14:279–284
- Bergstrom JS, Boyce MC (2001) Constitutive modeling of the time-dependent and cyclic loading of elastomers and application to soft biological tissues. *Mech Mater* 33:523–530
- Best TM, McElhaney J, Garret WE, Myers BS (1994) Characterization of the passive responses of live skeletal muscle using the quasilinear theory of viscoelasticity. *J Biomech* 27:413–419
- Bischoff JE, Arruda EM, Grosh K (2002) Orthotropic hyperelasticity in terms of an arbitrary molecular chain model. *J Appl Mech* 69:198–201
- Bischoff JE, Arruda EM, Grosh K (2004) A rheological network model for the continuum anisotropic and viscoelastic behavior of soft tissue. *Biomech Model Mechanobiol* 3:56–65
- Bischoff JE (2006) Reduced parameter formulation for incorporating fiber level viscoelasticity into tissue level biomechanical models. *Ann Biomed Eng* 34:1164–1172
- Boutouyrie P, Laurent S, Briet M (2008) Importance of arterial stiffness as cardiovascular risk factor for future development of new type of drugs. *Fundam Clin Pharmacol* 22:241–246
- Boyce BL, Jones RE, Nguyen TD, Grazier JM (2007) Stress-controlled viscoelastic tensile response of bovine cornea. *J Biomech* 40:2367–2376
- Cameron JD, Bulpitt CJ, Pinto ES, Rajkumar C (2003) The aging of elastic and muscular arteries: a comparison of diabetic and nondiabetic subjects. *Diabetes Care* 26:2133–2140
- Campa JS, Greenhalgh RM, Powell JT (1987) Elastin degradation in abdominal aortic aneurysms. *Atherosclerosis* 65:13–21
- Carew EO, Talman EA, Boughnew DR, Vesely I (1999) Quasi-linear viscoelastic theory applied to internal shearing of porcine aortic valve leaflets. *J Biomech Eng* 121:386–392
- Carew EO, Barber JE, Vesely I (2000) Role of preconditioning and recovery time in repeated testing of aortic valve tissues: validation through quasi-linear viscoelastic theory. *Ann Biomed Eng* 28:1093–1100
- Carew EO, Garg A, Barber JE, Vesely I (2004) Stress relaxation preconditioning of porcine aortic valves. *Ann Biomed Eng* 32:563–572
- Chung AW, Yang HH, Sigrist MK, Brin G, Chum E, Gourlay WA, Levin A (2009) Matrix metalloproteinase-2 and -9 exacerbate arterial stiffening and angiogenesis in diabetes and chronic kidney disease. *Cardiovasc Res*. doi:10.1093/cvr/cvp242
- Cox RH (1978) Passive mechanics and connective tissue composition of canine arteries. *Am J Physiol Heart Circ Physiol* 234:H533–H541
- Daamen WF, Veerkamp JH, van Hest JCM, van Kuppevelt TH (2007) Elastin as a biomaterial for tissue engineering. *Biomaterials* 28:4378–4398
- Diez J (2007) Arterial stiffness and extracellular matrix. *Adv Cardiol* 44:76–95
- Doehring TC, Carew EO, Vesely I (2004) The effect of strain rate on the viscoelastic response of aortic valve tissue: a direct-fit approach. *Ann Biomed Eng* 32:223–232
- Fonck E, Prod'homme G, Roy S, Augsburger L, Rufenacht DA, Stergiopoulos N (2007) Effect of elastin degradation on carotid wall mechanics as assessed by a constituent-based biomechanical model. *Am J Physiol Heart Circ Physiol* 292:H2754–H2763
- Fung YC (1993) *Biomechanics: mechanical properties of living tissues*. Springer, New York
- Geest JPV, Sacks MS, Vorp DA (2006) The effects of aneurysm on the biaxial mechanical behavior of human abdominal aorta. *J Biomech* 39:1324–1334
- Giles JM, Black AE, Bischoff JE (2007) Anomalous rate dependence of the preconditioned response of soft tissue during load controlled deformation. *J Biomech* 40:777–785
- Gosline JM (1976) The physical properties of elastic tissue. *Int Rev Connect Tissue Res* 7:211–249
- Grashow JS, Sacks MS, Liao J, Yoganathan AP (2006) Planar biaxial creep and stress relaxation of the mitral valve anterior leaflet. *Ann Biomed Eng* 34:1509–1518
- Guinea GV, Atienza JM, Elices M, Aragoncillo P, Hayashi K (2005) Thermomechanical behavior of human carotid arteries in the passive state. *Am J Physiol Heart Circ Physiol* 288:H2940–H2945
- Gundiah N, Ratcliffe MB, Pruitt LA (2009) The biomechanics of arterial elastin. *J Mech Behav Biomed Mater* 2:288–296
- Gundiah N, Ratcliffe MB, Pruitt LA (2007) Determination of strain energy function for arterial elastin: Experiments using histology and mechanical tests. *J Biomech* 40:586–594
- Guo X, Kassab GS (2004) Distribution of stress and strain along the porcine aorta and coronary arterial tree. *Am J Physiol Heart Circ Physiol* 286:H2361–H2368
- Hingorani RV, Provenzano PP, Lakes RS, Escarcega A, Vanderby RJr (2004) Nonlinear viscoelasticity in rabbit medial collateral ligament. *Ann Biomed Eng* 32:306–312
- Holzappel GA (2000) *Nonlinear solid mechanics: a continuum approach for engineering*. Wiley, Chichester
- Holzappel GA, Gasser TC, Stadler M (2002) A structural model for the viscoelastic behavior of arterial walls: continuum formulation and finite element analysis. *Eur J Mech A Solids* 21:441–463
- Huang CY, Wang VM, Flatow EL, Mow VC (2009) Temperature dependent viscoelastic properties of the human supraspinatus tendon. *J Biomech* 42:546–549
- Humphrey JD (2002) *Cardiovascular solid mechanics: cells, tissues, and organs*. Springer, New York
- Jhun CS, Evans MC, Barocas VH, Tranquillo RT (2009) Planar biaxial mechanical behavior of bioartificial tissues possessing prescribed fiber alignment. *J Biomech Eng* 131:081006
- Johnson GA, Tramaglino DM, Levine RE, Ohno K, Choi NY, Woo SL (1994) Tensile and viscoelastic properties of human patellar tendon. *J Orthop Res* 12:796–803
- Kang T, Resar J, Humphrey JD (1995) Heat-induced changes in the mechanical behavior of passive coronary arteries. *J Biomech Eng* 117:86–93
- Knauss WG, Emri IJ (1981) Non-linear viscoelasticity based on free volume consideration. *Comput Struct* 13:123–128
- Knezevic V, Sim AJ, Borg TK, Holmes JW (2002) Isotonic biaxial loading of fibroblast-populated collagen gels: a versatile, low-cost system for the study of mechanobiology. *Biomech Model Mechanobiol* 1:59–67
- Kwan MK, Li THD, Woo SLY (1993) On the viscoelastic properties of the anteromedial bundle of the anterior cruciate ligament. *J Biomech* 26:47–452
- Lally C, Reid AJ, Prendergast PJ (2004) Elastic behavior of porcine coronary artery tissue under uniaxial and equibiaxial tension. *Ann Biomed Eng* 32:1355–1364
- Liao J, Vesely I (2004) Relationship between collagen fibrils, glycosaminoglycans, and stress relaxation in mitral valve chordae tendinae. *Ann Biomed Eng* 32:977–983
- Liao J, Yang L, Grashow J, Sacks MS (2007) The relationship between collagen fibril kinematics and mechanical properties in the mitral valve anterior leaflet. *J Biomech Eng* 129:78–87
- Lillie MA, Gosline JM (1990) The effects of hydration on the dynamic mechanical properties of elastin. *Biopolymers* 29:1147–1160
- Lillie MA, Gosline JM (1996) Swelling and viscoelastic properties of osmotically stressed elastin. *Biopolymers* 39:641–693
- Lillie MA, Gosline JM (2002) The viscoelastic basis for the tensile strength of elastin. *Int J Biol Macromol* 30:119–127

- Lillie MA, Gosline JM (2007) Limits to the durability of arterial elastic tissue. *Biomaterials* 28:2021–2031
- Lu Q, Ganesan K, Simionescu DT, Vyavahare NR (2004) Novel porous aortic elastin and collagen scaffolds for tissue engineering. *Biomaterials* 25:5227–5237
- Lyerla JR Jr, Torchia DA (1975) Molecular mobility and structure of elastin deduced from the solvent and temperature dependence of ^{13}C magnetic resonance relaxation data. *Biochemistry* 14:5175–5183
- MacSweeney STR, Young G, Greenhalgh RM, Powell JT (1992) Mechanical properties of the aneurismal aorta. *Br J Surg* 79:1281–1284
- MacSweeney STR, Powell JT, Greenhalgh RM (1994) Pathogenesis of abdominal aortic aneurysms. *Br J Surg* 81:935–941
- Mow VC, Kuei SC, Lai WM, Armstrong CG (1980) Biphasic creep and stress relaxation of articular cartilage in compression: theory and experiments. *J Biomech Eng* 102:73–84
- Nagatomi J, Toosi KK, Chancellor MB, Sacks MS (2008) Contribution of the extracellular matrix to the viscoelastic behavior of the urinary bladder wall. *Biomech Model Mechanobiol* 7:395–404
- Nagatomi J, Gloeckner DC, Chancellor MB, DeGroat WC, Sacks MS (2004) Changes in the biaxial viscoelastic response of the urinary bladder following spinal cord injury. *Ann Biomed Eng* 32:1409–1419
- Nguyen TD, Jones RE, Boyce BL (2008) A nonlinear anisotropic viscoelastic model for the tensile behavior of the corneal stroma. *J Biomech Eng* 130:041020
- Öhman C, Baleani M, Viceconti M (2009) Repeatability of experimental procedures to determine mechanical behavior of ligaments. *Acta Bioeng Biomech* 11:19–23
- Provenzano P, Lakes R, Keenan T, Vanderby R Jr (2001) Nonlinear ligament viscoelasticity. *Ann Biomed Eng* 29:908–914
- Puso MA, Weiss JA (1998) Finite element implementation of anisotropic quasi-linear viscoelasticity using a discrete spectrum approximation. *J Biomech Eng* 120:62–70
- Sacks MS, Sun W (2003) Multiaxial mechanical behavior of biological materials. *Ann Rev Biomed Eng* 5:251–284
- Satta J, Laurila A, Pääkkö P, Haukipuro K, Sormunen R, Parkkila S, Juvonen T (1998) Chronic inflammation and elastin degradation in abdominal aortic aneurysm disease: an immunohistochemical and electron microscopic study. *Eur J Vasc Endovasc Surg* 15:313–319
- Sauren AAHJ, van Hout MC, van Steenhoven AA, Veldpaus FE, Janssen JD (1983) The mechanical properties of porcine aortic valve tissues. *J Biomech* 16:327–337
- Silver FH, Horvath I, Foran DJ (2001) Viscoelasticity of the vessel wall: the role of collagen and elastic fibers. *Crit Rev Biomed Eng* 29:279–301
- Soulhat J, Buschmann MD, Shirazi-Adl A (1999) A fibril-network-reinforced biphasic model of cartilage in unconfined compression. *J Biomech Eng* 121:340–347
- Spina M, Friso A, Ewins AR, Parker KH, Winlove CP (1999) Physicochemical properties of arterial elastin and its associated glycoproteins. *Biopolymers* 49:255–265
- Stella JA, Liao J, Sacks MS (2007) Time-dependent biaxial mechanical behavior of the aortic heart valve leaflet. *J Biomech* 40:3169–3177
- Stephens EH, Chu CK, Grande-Allen KJ (2008) Valve proteoglycan content and glycosaminoglycan fine structure are unique to microstructure, mechanical load and age: relevance to an age-specific tissue-engineered heart valve. *Acta Biomaterialia* 4:1148–1160
- Stergiopoulos N, Vulliamoz S, Rachev A, Meister J-J, Greenwald SE (2001) Assessing the homogeneity of the elastic properties and composition of the pig aortic media. *J Vasc Res* 38:237–246
- Sverdlik A, Lanir Y (2002) Time-dependent mechanical behavior of sheep digital tendons, including the effects of preconditioning. *J Biomech Eng* 124:78–84
- Thornton GM, Oliynyk A, Frank CB, Shrive NG (1997) Ligament creep cannot be predicted from stress relaxation at low stress: a biomechanical study of the rabbit medial collateral ligament. *J Orthop Res* 15:652–656
- Thornton GM, Frank CB, Shrive NG (2001) Ligament creep behavior can be predicted from stress relaxation by incorporating fiber recruitment. *J Rheol* 45:493–507
- Uitto J (1979) Biochemistry of the elastic fibers in normal connective tissues and its alterations in diseases. *J Invest Dermatol* 72:1–10
- von Maltzahn WW, Warriyar RG (1984) Experimental measurement of elastic properties of media and adventitia of bovine carotid arteries. *J Biomech* 17:839–847
- Weinberg PD, Winlove CP, Parker KH (1995) The distribution of water in arterial elastin: effects of mechanical stress, osmotic pressure, and temperature. *Biopolymers* 35:161–169
- Williams C, Liao J, Joyce EM, Wang B, Leach JB, Sacks MS, Wong JY (2009) Altered structural and mechanical properties in decellularized rabbit carotid arteries. *Acta Biomaterialia* 5:993–1005
- Winlove CP, Parker KH (1990) Connective tissue matrix II. In: Hukins DWL (ed) MacMillan, London, chap 7
- Yin FCP, Chew PH, Zeger SL (1986) An approach to quantification of biaxial tissue stress-strain data. *J Biomech* 19:27–37
- Zhang Y, Dunn ML, Drexler ES, McCowan CN, Slifka AJ, Ivy DD, Shandas R (2005) A microstructural hyperelastic model of pulmonary arteries under normo- and hypertensive conditions. *Ann Biomed Eng* 33:1042–1052
- Zou Y, Zhang Y (2009) An experimental and theoretical study on the anisotropy of elastin network. *Ann Biomed Eng* 37:1572–1583